UDC 621.9.048
DOI dx.doi.org/10.17073/1997-308X-2022-3-63-77

The effect of electrospark deposition using zirconium electrodes on structure and properties of nickel-containing alloy obtained selective laser melting

© 2022 г. **A.E. Kudryashov, Ph.V. Kiryukhantsev-Korneev, S.K. Mukanov, M.I. Petrzhik, E.A. Levashov**

National University of Science and Technology (NUST) «MISIS», Moscow, Russia

Received 14.03.2022, revised 09.06.2022, accepted for publication 15.06.2022

Abstract: Protective coatings were applied by electrospark deposition (ESD) using zirconium electrodes to improve the performance of the Ni-containing alloy obtained using the selective laser melting (SLM) technology. The kinetics of mass transfer was studied in 5 different frequency-energy processing modes. An analog-to-digital converter was used to determine the average number of pulse discharges, single-pulse energy, and the total energy of pulse discharges for 1 min of processing ($\sum E$) for all the modes used. In low-energy processing modes ($\sum E$ = 1459÷2915 J), a weak mass transfer was observed, and the cathode weight gain was recorded only in the first minutes. As the processing time increased, a decrease in the substrate weight was observed. The roughness of coatings (R_a) varied in the range of 3.9–7.2 μm. In high-energy modes ($\sum E$ = 5197÷17212 J), due to intense electrode heating, a steady cathode weight gain was observed, but the formed coatings featured by increased roughness: R_a = 7.4÷8.6 μm. The R_a parameter for the original SLM samples was 10.7 μm. The formed coatings featured by a thickness of 15–30 μm, high continuity (up to 100 %), hardness of 9.0–12.5 GPa, elastic modulus of 122–145 GPa, and friction coefficient of 0.36–0.49. The ESD processing promoted an increase in wear resistance of the SLM alloy by 7.5–20 times, and oxidation resistance by 10–20 % (t = 1150 °C, τ = 30 h). It was found that the coating obtained in the low-energy ESD mode with energy $\sum E$ = 2915 J featured the best performance (hardness, modulus of elasticity, roughness, wear resistance and oxidation resistance).

Keywords: electrospark deposition (ESD), selective laser melting (SLM), heat-resistant alloy, zirconium, hardness, oxidation resistance, wear resistance.

Kudryashov A.E. – Cand. Sci. (Eng.), Leading researcher of the Laboratory «In situ diagnostics of structural transformations», Scientific-Educational Center of SHS, MISIS–ISMAN, NUST «MISIS» (119049, Russia, Moscow, Leninskiy pr., 4).
E-mail: aekudr@yandex.ru.

Kiryukhantsev-Korneev Ph.V. – Cand. Sci. (Eng.), Associate prof., Department of powder metallurgy and functional coatings (PM&FC), NUST «MISIS»; Head of the Laboratory «In situ diagnostics of structural transformations», Scientific-Educational Center of SHS, MISIS–ISMAN.
E-mail: kiruhancev-korneev@yandex.ru.

Mukanov S.K. – Cand. Sci. (Eng.), Research assistant, Laboratory «In situ diagnostics of structural transformations», Scientific-Educational Center of SHS, MISIS–ISMAN. E-mail: sam-mukanov@mail.ru.

Petrzhik M.I. – Dr. Sci. (Eng.), Prof., Department of PM&FC, NUST «MISIS»; Leading researcher, Laboratory «In situ diagnostics of structural transformations», Scientific-Educational Center of SHS, MISIS–ISMAN.
E-mail: petrzhik@shs.misis.ru

Levashov E.A. – Dr. Sci. (Eng.), Prof., Acad. of Russian Academy of Natural Science; Head of the Department of PM&FC, NUST «MISIS»; Head of Scientific-Educational Center of SHS, MISIS–ISMAN.
E-mail: levashov@shs.misis.ru.

For citation: *Kudryashov A.E., Kiryukhantsev-Korneev Ph.V., Mukanov S.K., Petrzhik M.I., Levashov E.A*. The effect of electrospark deposition using zirconium electrodes on structure and properties of nickel-containing alloy obtained selective laser melting. *Izvestiya Vuzov. Poroshkovaya Metallurgiya i Funktsional'nye Pokrytiya (Powder Metallurgy and Functional Coatings)*. 2022. Vol. 16. No. 3. P. 63–77 (In Russ.).
DOI: dx.doi.org/10.17073/1997-308X-2022-3-63-77.

Влияние электроискровой обработки электродами из циркония на структуру и свойства никельсодержащего сплава, полученного селективным лазерным сплавлением

А.Е. Кудряшов, Ф.В. Кирюханцев-Корнеев, С.К. Муканов, М.И. Петржик, Е.А. Левашов

Национальный исследовательский технологический университет (НИТУ) «МИСиС», г. Москва, Россия

Статья поступила в редакцию 14.03.2022 г., доработана 09.06.2022 г., подписана в печать 15.06.2022 г.

Аннотация: Для повышения эксплуатационных свойств Ni-содержащего сплава, полученного по технологии селективного лазерного сплавления (СЛС), наносили защитные покрытия методом электроискрового легирования (ЭИЛ) с использованием электродов из циркония. Кинетику массопереноса изучали на 5 различных частотно-энергетических режимах обработки. С помощью аналого-цифрового преобразователя установлены среднее количество импульсных разрядов, энергия единичных импульсов и суммарная энергия импульсных разрядов за 1 мин обработки ($\sum E$) для всех применяемых режимов. В низкоэнергетических условиях обработки ($\sum E$ = 1459÷2915 Дж) наблюдался слабый массоперенос, привес массы катода фиксировался только в первые минуты. С увеличением времени обработки происходила убыль массы подложки. Шероховатость покрытий (R_a) варьировалась в диапазоне 3,9–7,2 мкм. На высокоэнергетических режимах ($\sum E$ = 5197÷17212 Дж) из-за интенсивного нагрева электродов наблюдался устойчивый привес массы катода, но сформированные покрытия имели повышенную шероховатость: R_a = 7,4÷8,6 мкм. Параметр R_a для исходных СЛС-образцов составлял 10,7 мкм. Сформированные покрытия характеризовались толщиной 15–30 мкм, высокой сплошностью (до 100 %), твердостью 9,0–12,5 ГПа, модулем упругости 122–145 ГПа, коэффициентом трения 0,36–0,49. Проведение ЭИЛ-обработки способствовало росту износостойкости СЛС-сплава в 7,5–20,0 раз, а жаростойкости на 10–20 % (t = 1150 °С, τ = 30 ч). Установлено, что наилучшими свойствами (твердость, модуль упругости, шероховатость износо- и жаростойкость) обладает покрытие, полученное на низкоэнергетическом режиме ЭИЛ с энергией $\sum E$ = 2915 Дж.

Ключевые слова: электроискровое легирование (ЭИЛ), селективное лазерное сплавление (СЛС), жаропрочный сплав, цирконий, твердость, жаростойкость, износостойкость.

Кудряшов А.Е. – канд. техн. наук, вед. науч. сотрудник лаборатории «In situ диагностика структурных превращений», НУЦ СВС, МИСиС–ИСМАН, НИТУ «МИСиС» (119049, г. Москва, Ленинский пр-т, 4, стр. 1).
E-mail: aekudr@yandex.ru.

Кирюханцев-Корнеев Ф.В. – канд. техн. наук, доцент кафедры порошковой металлургии и функциональных покрытий (ПМиФП), НИТУ «МИСиС»; зав. лабораторией «In situ диагностика структурных превращений», НУЦ СВС, МИСиС–ИСМАН.
E-mail: kiruhancev-korneev@yandex.ru.

Муканов С.К. – канд. техн. наук, мл. науч. сотрудник лаборатории «In situ диагностика структурных превращений», НУЦ СВС, МИСиС–ИСМАН. E-mail: sam-mukanov@mail.ru.

Петржик М.И. – докт. техн. наук, профессор кафедры ПМиФП, НИТУ «МИСиС»; вед. науч. сотрудник лаборатории «In situ диагностика структурных превращений», НУЦ СВС, МИСиС–ИСМАН.
E-mail: petrzhik@shs.misis.ru.

Левашов Е.А. – докт. техн. наук, акад. РАЕН, проф., зав. кафедрой ПМиФП, НИТУ «МИСиС»; директор НУЦ СВС, МИСиС–ИСМАН.
E-mail: levashov@shs.misis.ru.

Для цитирования: *Кудряшов А.Е., Кирюханцев-Корнеев Ф.В., Муканов С.К., Петржик М.И., Левашов Е.А.* Влияние электроискровой обработки электродами из циркония на структуру и свойства никельсодержащего сплава, полученного селективным лазерным сплавлением. *Известия вузов. Порошковая металлургия и функциональные покрытия.* 2022. Т. 16. No. 3. С. 63–77.
DOI: dx.doi.org/10.17073/1997-308X-2022-3-63-77.

Introduction

Advanced aerospace engineering requires new materials and technologies. New heat-resistant materials, also nickel-based, are currently under development [1, 2].

The most promising are additive technologies [3] such as selective laser melting (SLM). However, products manufactured by the SLM method are characterized by near-surface structural defects, among them cracks, pores, and non-molten particles are the most dangerous [4].

Applying a protective coating is the most efficient way to extend the service life of heat-resistant alloys [5—8]. Ion plasma deposition [9, 10], gas thermal sputtering [11—13], slip molding [14], and electrospark deposition (ESD) [15—20] are widely used for coating deposition on Ni-containing alloys.

The ESD advantages consist of good adhesion of the coating, relative simplicity of the process and equipment, low energy consumption, sustainability, high-profit margin, and many automation options. High-energy electrospark deposition successfully used to restore worn-out parts.

ESD on the ZhS6U nickel alloy with an electrode made of KhTN-61 alloy (Co—Cr—Nb) improves the oxidation resistance (up to 1000 °C), wear resistance, increases hardness, and reduces the friction coefficient [17]. Electrospark deposition of (Cr—Al—Si—B) electrodes obtained by Self propagated High temperature Synthesis (SHS) on the EP 718-ID (Inconel 718) heat-resistant nickel alloy can also increase the heat and wear resistance [18]. Kudryashov A.E. et al. [19, 20] report the increase of the EP 718-ID alloy oxidation resistance after deposition of SHS electrodes (Mo—Si—B and Zr—Si—B).

Tsyvirko E.I. et al. [21] note an improvement in the physical properties of critical aircraft castings made of nickel alloys when alloyed with 2—3 % Zr. Adding zirconium (0.05—0.25 %) to nickel alloys increases the microhardness of the metal matrix and improves the heat resistance of cast jet engine parts. Adding zirconium and hafnium to nickel alloys increases the oxide layer adhesion to the surface due to lower porosity at the oxide-alloy interface [22].

In view of the above, the investigation of the electrospark deposition of Ni-containing SLM alloy with zirconium electrodes is particular interest. It is expected that ESD will improve oxidation resistance and eliminate surface defects [16].

Multicomponent Zr-containing electrodes are extensively used. For example, CLAB 2 (ZrB_2—$ZrSi_2$—LaB_6) composite with the Ni—Cr—Al binder (30 mol.%) [23] and a $ZrSiO_4$ electrode [24] is used to increase the oxidation resistance of hard metal. In order to improve the wear resistance of the TC11 titanium alloy, the high-entropic CuNiSiTiZr [25] as well as the bulk metallic glass forming the $Zr_{65}Cu_{17,5}Al_{7,5}Ni_{10}$ electrodes [26, 27] were used. Vitreloy 1 ($Zr_{41.2}Ti_{13.8}Ni_{10}Cu_{12.5}Be_{22.5}$) was proposed for welds repairs in worn-out amorphous materials and coatings [28]. To protect the AISI 304 stainless steel against wear, corrosion and tribocorrosion ESD has done in a vacuum with a TaC—ZrC—Mo—Ni electrode [29]. Verkhoturov A.D. et al., Nikolenko S.V. et al. [30, 31] recommend using zirconium only as an electrode binder.

Despite the widespread use of multicomponent Zr-containing electrodes, the application of pure zirconium is limited. In order to improve the quality of Kh12MF steel grade die tooling, we propose the addition of ESD of zirconium first, and then an induction chemical and thermal treatment in a carbon-containing paste [32].

Nikolenko S.V. et al. [33] propose the use of zirconium as an anode material for the treatment of the VT20 titanium alloy, in order to improve its wear and oxidation resistance, or to extend the cutting tool life [34].

This study considers mass transfer, structure, composition, and properties of electrospark deposition of zirconium electrodes on a Ni-containing SLM alloy.

Materials and Methods

The Ni-containing SLM alloy served as a substrate (cathode). Its composition was (wt.%): Ni: 53.75, Al: 24.07, Cr: 13.73, Co: 7.66, Hf: 0.79 [35]. The sample size was 7 mm × 9 mm × 7 mm.

The electrode (anode) was made of zirconium iodide (TU 95 46-97 specifications) with the following composition (wt.%): Zr: base metal, Fe: 0.03, Cu: 0.003, Ni: 0.01, C: 0.008, Si: 0.008, N: 0.005, O: 0.05, Al: 0.005, Cr: 0.002, Hf: 0.01, B: 0.00005, Ti: 0.005. The sample size was 3 mm × 3 mm × 50 mm.

We used an Alier-Metal 303, Alier-Metal 30, and an

Table 1. **Parameters of ESD processing modes**

Таблица 1. Параметры режимов ЭИЛ-обработки

Mode	Alier-Metal machine	Amperage I, A	Pulse duration τ, μs	Pulse frequency f, Hz	N_{avg}	E_{avg}, 10^{-3} J	ΣE, J
1	303	120	20	3 000	66 895	43.57	2915
2	30	170	25	3 000	128 764	133.67	17212
3	30	170	25	1 500	49 829	104.29	5197
4	2002	340	6	15 000	262 803	5.55	1459
5	2002	340	8	10 000	257 270	10.27	2642
Note. The electrode vibration frequency was 600 Hz.							

Alier-Metal 2002 (METAL — SCINTI SRL, Russia—Moldova) ESD machines using 5 different frequency and power settings (refer to Table 1).

The surface layer was deposited in an argon environment (99.995 %). After treatment, the electrode and substrate were held in an argon bath until complete cooling.

We used a fast analog to digital converter (ADC) E20-10 (L-Card, Russia) connected to the ESD machine, in order to measure the properties of the pulsed discharges. The raw data was logged by the LGraph 2 software multichannel logger. The recording time was 10 sec. We also used MATLAB configured to handle the ESD process to estimate the energy of a single pulse discharge (E), the number of pulses (N), and the total energy per 1 minute of treatment (ΣE).

We used a KERN 770 (Germany) analytical balance to evaluate the mass transfer kinetics (anode's specific erosion ΔA_i) and cathode specific weight gain (ΔK_i)). The accuracy was 10^{-5} g. We weighed the anode and cathode after each minute of ESD. The total cathode weight gain is [30]

$$\Sigma\Delta K_i = (\Delta K_1 + \Delta K_2 + ... + \Delta K_{10}) / \rho, \quad (1)$$

where ΔK_i is the cathode weight gain in i min of deposition (i = 1, 2...10, g); ρ is the electrode material density, g/cm^3.

The anode total erosion $\Sigma\Delta A_i$ was estimated similarly.

We used a CitoPress-1 mounting press (Struers, Denmark) to embed the samples into conductive resin and make sample sections. A RotoPol-21 polishing machine (Struers) was used to grind and polish the samples. Initially, the samples were polished with various sandpaper grits. We polished the samples with a SiO_2 oxide suspension, 0.05 μm abrasive particle size. The metallographic analysis of the sections was performed with a Neophot-32 optical microscope (Carl Zeiss, Germany). The magnifications for measuring the thickness and continuity of the coatings were 500$^\times$ and 200$^\times$, respectively.

XRD patterns of the electrospark deposition coatings were performed on a DRON 4 diffractometer using monochromatic CuK_α radiation in the step-scanning mode, $2\theta = 10^\circ \div 110^\circ$ angular range (the scanning step was 0.1°, the exposure was 3 to 6 s). The qualitative and quantitative phase analysis procedures are given in [36, 37].

We studied the sample microstructures by scanning electron microscopy (SEM) using an S-3400N microscope (Hitachi, Japan) using a NORAN 7 spectral imaging X-ray microanalysis system (Thermo Fisher Scientific Inc, USA). The sample surface topography and wear tracks were examined using a WYKO NT 1100 optical profiler (VEECO, USA).

The mechanical properties such as hardness (H) and modulus of elasticity (E) were determined by indentation of polished cross sections at the Functional Surfaces Testing Lab, National University of Science and Technology «MISIS», using a Nano-Hardness Tester (CSM Instruments, Switzerland) with a Berkovich diamond tip. We determined H and E according to GOST R 8.748-2011 (ISO 14577) [38]. The Poisson's ratio was assumed to be 0.3. The measurement conditions were as follows: 20 mN max load, 5 s hold time.

The study of tribological properties of samples was carried out on an friction machine Tribometer (CSM Instruments) according to the pin-on-plate scheme with

reciprocating motion. A ball with a diameter of 3 mm made of WC—Co alloy was used as a static partner. Test conditions: track length 4 mm, applied load 1 N, maximum velocity 5 cm/s.

The oxidation resistance of the coatings was evaluated by the sample weight gain after annealing in the air in a SNOL 7.2/1200 electric furnace at 1150 °C, with 30 h total dwell time.

Results and Discussion

Fig. 1 shows the total anode erosion ($\Sigma\Delta A_i$) and total cathode weight gain ($\Sigma\Delta K_i$) depending on ESD time. It was found that $\Sigma\Delta A_i$ increases with processing time for all process modes. The max value ($-73.17\cdot10^{-4}$ cm^3) is reached in High-Energy Mode 2.

The peculiarities of the dependences of the total cathode gain on the time is determined by the processing mode used.

For example, when low-energy modes were used (samples *1*, *4*, *5*), we observed initial cathode weight gain. The initial weight gain period varied from 1 min (mode *4*) to 3 and 4 min in modes *5* and *1*, respectively. As the processing time increases, the substrate loses weight. The min value $\sum\Delta K_i = -5.81\cdot10^{-4}$ cm^3 was found after a 10 min mode *4* deposition.

In high-energy modes *2* and *3*, there is a consistent cathode weight gain. Due to intense electrode heating, burns occur on the surfaces, leading to strong deterioration of the surface finish. Such surfaces would require extra grinding. To avoid burns, the processing time was reduced to 5 min. In modes *2* and *3* $\sum\Delta K_i$ was $59.03\cdot10^{-4}$ and $22.42\cdot10^{-4}$ cm^3, respectively.

For comparison, when using a ZrSiB electrode (composition, wt.%: ZrB_2: 66, $ZrSi_2$: 26, Si: 6, ZrO_2: 2) to treat the EP718 alloy in mode *1*, the following values were observed: $\sum\Delta K_i = 10.01\cdot10^{-4}$ cm^3, and $\sum\Delta A_i = -43.43\cdot10^{-4}$ cm^3 [20]. The mass transfer is intensified since the ESD erosion of refractory substances is an order of magnitude higher than that of metals due to their mostly brittle fracturing [30].

We analyzed the ADC logs which included the single pulse energy (average values over processing time (E_{avg})), the total energy of pulse discharges per 1 min ($\sum E$), and the average number of pulse discharges per 1 min in each mode (N_{avg})) (refer to Table 1).

It was found that in mode *2*, $\sum E$ is at its maximum: 17212 J. In mode *4* with its short, max frequency pulse discharges, the total energy is at its minimum: 1459 J.

Low-energy treatment leads to a low coating formation rate. In high-energy modes, the electrodes are

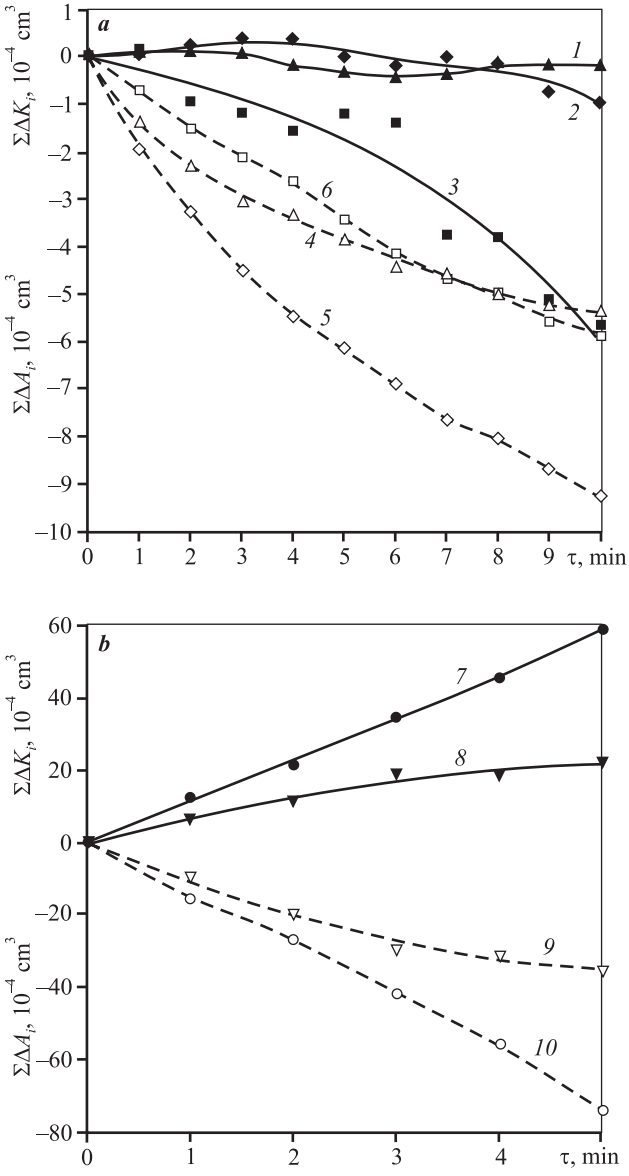

Fig. 1. Total anode erosion $\Sigma\Delta A_i$ (dashed lines, light symbols) and total cathode weight gain $\Sigma\Delta K_i$ (solid lines, dark symbols) depending on ESD time

Curves ***1***, ***4*** – Mode 5 (▲, △); ***2***, ***5*** – Mode 1 (◆, ◇); ***3***, ***6*** – Mode 4 (■, □); *7*, ***10*** – Mode 2 (●, ○); ***8***, ***9*** – Mode 3 (▼, ▽)

Рис. 1. Зависимость суммарной эрозии анода $\Sigma\Delta A_i$ (штриховые линии, светлые значки) и суммарного привеса катода $\Sigma\Delta K_i$ (сплошные линии, темные значки) от времени ЭИЛ

Кривые ***1***, ***4*** – 5-й режим (▲, △); ***2***, ***5*** – 1-й (◆, ◇); ***3***, ***6*** – 4-й (■, □); *7*, ***10*** – 2-й (●, ○); ***8***, ***9*** – 3-й (▼, ▽)

intensively heated. In this case the ESD performance is high, but the surface roughness of the coatings is unsatisfactory.

We found the optimal ESD processing time per 1 cm^2 for the coating application on SLM alloy samples. It is 4 min for the low-energy modes (*1*, *4*, *5*) and 1 min for the high-energy modes (*2*, *3*). This time is sufficient to build solid coatings with an acceptable surface finish. Refer to Table 2 for the R_a (arithmetic average roughness) surface roughness. It is clear that ESD reduces the SLM alloy surface roughness by 1.3—2.8 time. Coating *1* featured the min roughness.

Table 3 lists the phase composition of the coatings. It was found that the SLM alloy contains only the NiAl intermetallic. Coating *1* contains nickel aluminides (NiAl), lattice parameter a = 0.2886 and 0.2922 nm. Its increase may be caused by the introduction of Zr atoms into NiAl during ESD (composition: $Al_{11.45}Ni_{49.83}Zr_{38.72}$). This sample also contains the $ZrNi_2Al$ intermetallic and Zr(OH). Its formation appears to be caused by the interaction between zirconium and dissolved oxygen in the SLM samples. Coating *2* was manufactured with the highest ESD energy possible. It contains NiAl and ZrNi intermetallics, as well as the $Zr_3NiO(x)$ oxide. In addition to sample *1*, the $ZrNi_2Al$ was also found in coatings *3* and *4*. They contain the $ZrCr_2$ phase as well. The $ZrNi_2Al$ triple intermetallic compound is a Heusler phase while the $ZrCr_2$ double intermetallic compound is a Laves phase. The formation of both phases is caused by the interaction between zirconium (anode) and the substrate elements during ESD.

It should be noted that zirconium oxynitride Zr(O, N) with the lattice parameter a = 0.4585 nm corresponds to $Zr_{85.56}N_{3.94}O_{10.5}$ (wt.%). The double oxide $Zr_3NiO(x)$ can be expressed as $Zr_{80.86}Ni_{17.34}O_{1.8}$ (a = 0.329 nm, b = 10.94 nm, c = 8.91 nm).

$ZrCr_2$ melting point is known to be t = 1673 °C [40], and the ZrNi phase melting point is 1260 °C [41]. The formation of such refractory phases should improve the oxidation resistance of the coating.

Fig. 2 shows the SEM images of the ESD coatings *1* and *3*. It can be seen that the surface layer is continuous. It consists of the spread electrode material drops. In the case of high-energy mode *2*, the drop diameter is ~ 450 μm, for high-frequency mode *5*, it is about 170 μm.

Fig. 3, *a* shows an SEM image of coating *5* (polished section). It can be seen that ESD generates a defect-free coating. No cracks at the coating/substrate interface were found.

Electrospark deposition forms a highly continuous (up to 100 %) coating up to 30 μm thick (h) on the surface of an SLM alloy.

Our nano-indentation measurements estimated the mechanical properties of the coatings: E = 122÷145 GPa and H = 9.0÷12.5 GPa (refer to Table 2). The modulus of elasticity of the unhardened sample is higher than that of the electrospark coating and zirconium (96.0—99.0 GPa [42]). The reason is the interaction between Zr and the substrate elements during ESD.

ESD increases the surface hardness by 1.3—1.8 time. Fig. 3, *b* shows the hardness and modulus of elasticity vs. the cross-section width for coating *5*. It can be seen that as the distance to the surface increases, H decreases, and E increases.

When using a ZrSiB electrode to treat the EP718 alloy, the coating has higher hardness (18.8 GPa), modulus of elasticity (351.4 GPa), and roughness (R_a = 5.80 μm) [20]. The max coating hardness of 9.2 GPa was obtained

Table 2. **Properties of the substrate and ESD coatings**

Таблица 2. Свойства подложки и ЭИЛ-покрытий

Sample (mode)	h, μm	R_a, μm	E, GPa	H, GPa
Substrate	–	10.7	162	6.9
1	15	3.9	140	12.3
2	20	8.6	122	9.0
3	30	7.4	145	12.5
4	15	5.0	136	11.1
5	15	7.2	142	10.7

Table 3. **Phase composition of the substrate and ESD coatings**

Таблица 3. Фазовый состав подложки и ЭИЛ-покрытий

Sample (mode)	Phase	Lattice type	Space group	Vol. fraction, %	Mass fraction, %	Lattice constants, nm
Substrate	NiAl	*B*2	*cP*2/1	100	100	$a = 0.2880$
1	NiAl	*B*2	*cP*2/1	45	44	$a = 0.2886$
	NiAl(Zr)	*B*2	*cP*2/1	2	30	$a = 0.2922$
	$ZrNi_2Al$	*D*0.3	*cF*16/2	9	10	$a = 0.6034$
	Zr (O,N)	*B*1	*cF*8/2	14	16	$a = 0.4656$
2	NiAl	*B*2	*cP*2/1	17	15	$a = 0.2877$
	ZrNi	*E*9.3	*cF*96/1	36	37	$a = 1.1985$
	$Zr_3NiO(x)$	*E*1*a*	*oC*20/7	47	48	$a = 3.304$ $b = 11.128$ $c = 8.679$
3	NiAl	*B*2	*cP*2/1	68	64	$a = 0.2881$
	$ZrCr_2$	*C*14	*hP*12/1	13	15	$a = 0.5032$ $c = 0.8328$
	$ZrNi_2Al$	*D*0.3	*cF*16/2	10	11	$a = 0.6023$
	Zr (O,N)	*B*1	*cF*8/2	9	10	$a = 0.4637$
4	NiAl	*B*2	*cP*2/1	51	47	$a = 0.2879$
	$ZrCr_2$	*C*14	*hP*12/1	22	24	$a = 0.5046$ $c = 0.8206$
	$ZrNi_2Al$	*D*0.3	*cF*16/2	13	14	$a = 0.6045$
	Zr (O,N)	*B*1	*cF*8/2	14	15	$a = 0.4646$
5	NiAl	*B*2	*cP*2/1	37	33	$a = 0.2882$
	Zr (O,N)	*B*1	*cF*8/2	38	41	$a = 0.4650$
	$Zr_3NiO(x)$	*E*1*a*	*oC*20/7	25	26	$a = 3.321$ $b = 11.118$ $c = 8.679$

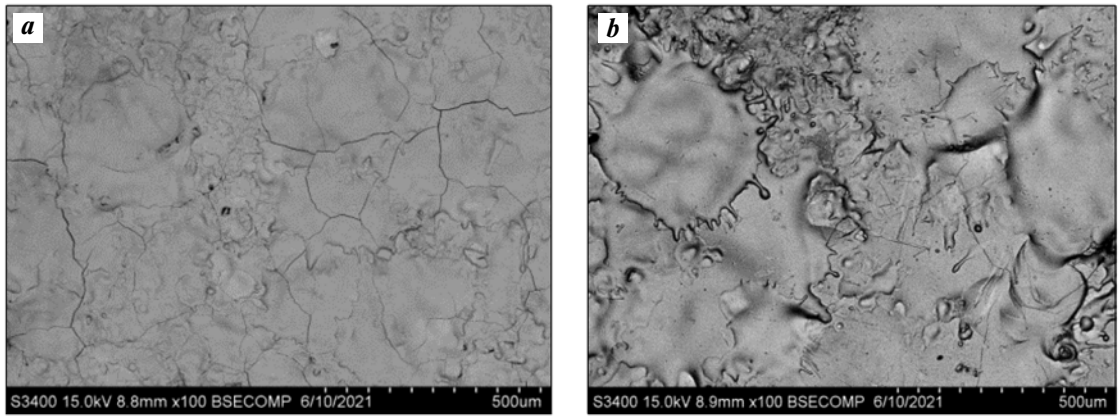

Fig. 2. SEM images of surfaces of ESD coating samples *1* (***a***) and *3* (***b***)

Рис. 2. РЭМ-изображения поверхности образцов ЭИЛ-покрытий *1* (***a***) и *3* (***b***)

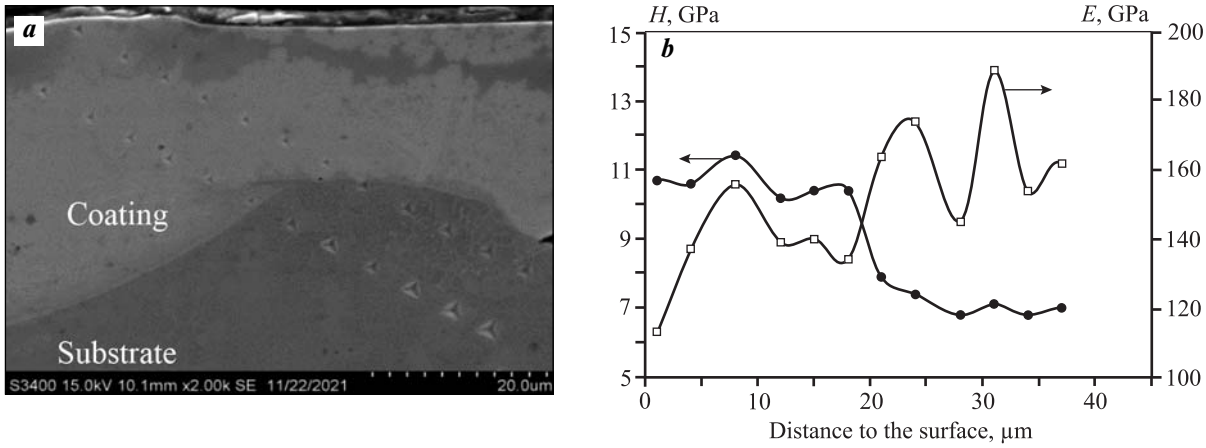

Fig. 3. SEM image of Coating *5* cross-section (***a***) and hardness (*H*) and elastic modulus (*E*) distribution over the coating thickness (***b***)

Рис. 3. РЭМ-изображение поперечного шлифа покрытия *5* (***a***) и распределение твердости (*H*) и модуля упругости (*E*) по его толщине (***b***)

after vacuum treatment of the EP 741 nickel alloy with a NiAl-based alloy electrode [43].

Table 4 lists the tribology test results (friction coefficient (K_{fr}) and reduced wear) for the substrate and ESD coatings. It was found that the unhardened sample has a minimum value of $K_{fr} = 0.34$. ESD increases the friction coefficient: for ESD coatings, $K_{fr} = 0.36 \div 0.49$.

The min friction coefficient of 0.36 was found in sample *4*. Coating *2* was applied in a high-energy mode. At the beginning of testing (up to 5500 cycles) the friction coefficient $K_{fr} \sim 0.33$ was low, and by the end (7000 cycles), it rose to 0.49. Apparently, during the test, the solid wear products on the track surface were able to enter the friction zone thus increasing the friction coefficient [44].

The friction coefficient of the coating formed by the KhTN-61 electrode on the EP718 heat-resistant nickel alloy ($E = 0.3$ J, $f = 1000$ Hz, $\tau = 50$ μs) is $K_{fr} = 0.18$. The value is so low because the surface layer was polished [17].

An unhardened sample of a Ni-containing alloy (Table 4) was found to have the max reduced wear (that is, min wear resistance). Electrospark deposition with a zirconium electrode reduces the reduced wear. Coating *1* showed the best results.

The tribology tests produced cracks on the track surface of the unhardened sample. A possible reason is the shear stresses under load. Samples with coatings *1*, *2*, *3*, and *5* featured partial wear. On these coatings Zirconium was found at the bottom of the tracks. Its content on the sample surface was noticeably higher.

No zirconium was found at the bottom of the wear track in coating *4*, manufactured in the high-frequency mode (15000 Hz), with the min $K_{fr} = 0.36$ and max specific wear rate of $44.4 \cdot 10^{-5}$ mm^3/(N·m). This indicates that the coating is completely worn out.

Fig. 4 shows the oxidation weight index ($\Delta m/S$) as a function of time for the ESD coatings and the unhardened substrate. It was found that oxidation follows the parabolic law, and the oxide layer growth is limited by the oxygen diffusion through it. The maximum coating oxidation rate is observed in the first minutes of the experiment. It reduces after the formation of an oxidized layer on the sample surface.

Fig. 4 shows that coating *3* ($\Delta m/S = 527.62$ g/m^2) and the unhardened sample ($\Delta m/S = 520.68$ g/m^2) have the lowest oxidation resistance, while sample1 showed the best results ($\Delta m/S = 434.90$ g/m^2).

The application of ESD coatings reduces the weight oxidation index by 10—20 %. The oxidation resistance seems to be caused both by the reduction of the SLM alloy surface defects and the formation of a more heat-resistant surface layer.

Table 5 lists the phase composition of the substrate and ESD coatings after long (30 h total time), high-temperature treatment. The following phases were found in the unhardened sample: NiAl (45 %), double oxide $(Al,Cr)_2O_3$ (46 %), traces of HfO_2 (4 %), and $NiCrO_3$ (5 %).

Table 4. **Tribology test results for the substrate and ESD coatings**

Таблица 4. Результаты трибологических испытаний подложки и ЭИЛ-покрытий

Sample (mode)	Reduced wear, 10^{-5} mm^3/(N·m)	K_{fr}			
		Initial	Max.	Avg.	Final
Substrate	142.0	0.02	0.37	0.30	0.34
1	7.0	0.22	0.49	0.44	0.44
2	12.5	0.26	0.50	0.30	0.49
3	18.4	0.65	0.44	0.38	0.41
4	44.4*	0.06	0.45	0.38	0.36
5	14.6	0.11	0.46	0.39	0.42

* The coating is completely gone.

All the coated samples contain NiAl, and the oxides of the substrate elements: $(Al,Cr)_2O_3$, Co_3O_4, $NiCrO_3$ (traces), and zirconium dioxide (ZrO_2), present as two modifications: monoclinic lattice (*C*43), 7 to 28 %, and HCC lattice (*C*1), not more than 2 %.

The presence of $(Al,Cr)_2O_3$ and ZrO_2 oxides in the coatings is desirable. A thin $(Al,Cr)_2O_3/ZrO_2$ coating made by arc ion sputtering on a nickel-based superalloy is known to have high oxidation resistance at t = = 1200 °C, and provides good thermal insulation. At the 1100 °C ambient temperature, the substrate temperature decreased by more than 40 °C [45].

Fig. 5 shows the substrate cross section after long annealing, and an element distribution chart (O, Al, Ni). It can be seen that high-temperature annealing forms a 30 μm thick nickel-free oxidized layer on the substrate surface.

Fig. 6 shows a thin section of coating *4* after annealing and an element distribution chart (O, Zr, Al, Ni) in the oxidized layer. It was found that the surface layer (region *1*) mostly contains zirconium and oxygen, the middle layer (region *2*) contains oxygen, substrate material (Al, Ni, Cr, Co), and electrode (Zr) elements, while the bottom layer (region *3*) contains O, Al, Cr, and small amounts (≤ 1 %) of Ni and Zr. The total thickness of the oxide layers does not exceed 9 μm.

Prolonged high-temperature annealing results in the diffusion of the surface layer elements. The top layer is Zr-containing. The bottom layer bordering the substrate contains aluminum and chromium oxides. The middle layer contains chromium, nickel, and hafnium oxides besides aluminum oxide. For all the coatings the total thickness of oxide layers does not exceed

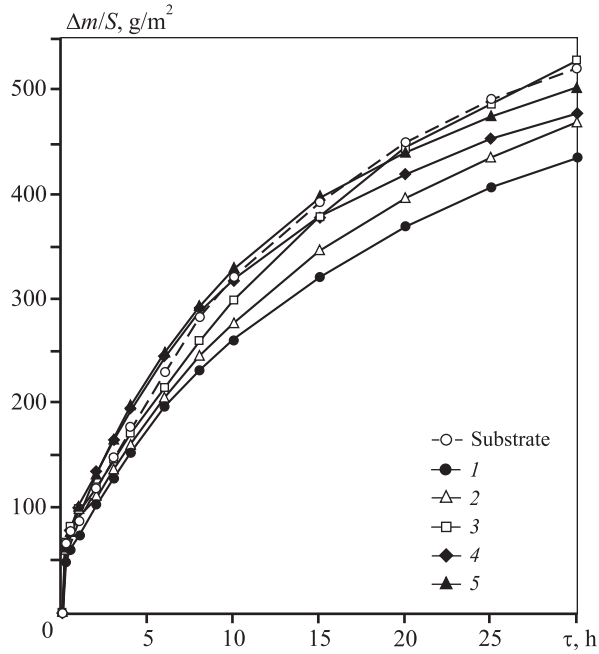

Sample (mode)	Regression equation	Approximation confidence coefficient
Substrate	$\Delta m/S = 97.397\tau^{0,5}$	0.9982
1	$\Delta m/S = 80.920\tau^{0,5}$	0.9992
2	$\Delta m/S = 86.761\tau^{0,5}$	0.9987
3	$\Delta m/S = 95.631\tau^{0,5}$	0.9979
4	$\Delta m/S = 93.648\tau^{0,5}$	0.9968
5	$\Delta m/S = 94.597\tau^{0,5}$	0.9934

Fig. 4. Oxidation weight indicator of the substrate (dashed line) and coatings (solid curves) as a function of time

Curve numbers correspond to the numbers of coating samples (modes)

Рис. 4. Зависимость весового показателя окисления подложки (штриховая линия) и покрытий (сплошные кривые) от времени

Цифры у кривых соответствуют номерам образцов покрытий (режимам)

Table 5. **Phase composition of the substrate and ESD coatings after annealing**

Таблица 5. Фазовый состав подложки и ЭИЛ-покрытий после отжига

Sample (mode)	Phase	Lattice type	Space group	Vol. fraction,%	Mass fraction,%	Lattice constants, nm Lattice angle β, deg
Substrate	NiAl	*B*2	*cP*2/1	39	45	$a = 0.2873$
	HfO_2	*C*43	*mP*12/3	2	4	–
	$(Al,Cr)_2O_3$	*D*5.1	*hR*10/1	54	46	$a = 0.476$ $c = 1.3025$
	$NiCrO_3$	*D*5.1	*hR*10/1	5	5	–
1	ZrO_2	*C*43	*mP*12/3	6	7	–
	Ni Al	*B*2	*cP*2/1	32	35	$a = 0.2869$
	$(Al,Cr)_2O_3$	*D*5.1	*hR*10/1	35	29	$a = 0.4766$ $c = 1.3016$
	$NiCrO_3$	*D*5.1	*hR*10/1	5	5	–
	ZrO_2	*C*1	*cF*12/1	2	2	$a = 5.136$
	Co_3O_4		*cF*56/3	20	22	$a = 0.8120$
2	ZrO_2	*C*43	*mP*12/3	26	28	$a = 0.5150$ $b = 0.5199$ $c = 0.5327$ $\beta = 99.09°$
	NiAl	*B*2	*cP*2/1	19	22	$a = 0.2869$
	$(Al,Cr)_2O_3$	*D*5.1	*hR*10/1	39	32	$a = 0.4771$ $c = 1.3030$
	$NiCrO_3$	*D*5.1	*hR*10/1	4	4	–
	ZrO_2	*C*1	*cF*12/1	1	1	$a = 0.5127$
	Co_3O_4		*cF*56/3	11	13	$a = 0.8120$
3	ZrO_2	*C*43	*mP*12/3	12	13	$a = 0.5155$ $b = 0.5175$ $c = 0.5329$ $\beta = 99.10°$
	NiAl	*B*2	*cP*2/1	23	26	$a = 0.2870$
	$(Al,Cr)_2O_3$	*D*5.1	*hR*10/1	44	37	$a = 0.477$ $c = 1.3028$
	$NiCrO_3$	*D*5.1	*hR*10/1	4	5	–
	Co_3O_4		*cF*56/3	17	19	$a = 0.8125$
4	ZrO_2	*C*43	*mP*12/3	14	15	$a = 0.5146$ $b = 0.5188$ $c = 0.5322$ $\beta = 99.16°$
	Ni Al	*B*2	*cP*2/1	26	28	$a = 0.2870$
	$(Al,Cr)_2O_3$	*D*5.1	*hR*10/1	38	32	$a = 0.4770$ $c = 1.3023$
	$NiCrO_3$	*D*5.1	*hR*10/1	5	5	–
	ZrO_2	*C*1	*cF*12/1	1/1	1	$a = 0.5132$
	Co_3O_4		*cF*56/3	16	19	$a = 0.8114$

Table 5. **Phase composition of the substrate and ESD coatings after annealing (the ending)**

Таблица 5. Фазовый состав подложки и ЭИЛ-покрытий после отжига (окончание)

Sample (mode)	Phase	Lattice type	Space group	Vol. fraction,%	Mass fraction,%	Lattice constants, nm Lattice angle β, deg
5	ZrO_2	*C*43	*mP*12/3	16	17	*a* = 0.5147 *b* = 0.5195 *c* = 0.5331 β = 99.19°
	Ni Al	*B*2	*cP*2/1	27/31	31	*a* = 0.2871
	$(Al,Cr)_2O_3$	*D*5.1	*hR*10/1	40	33	*a* = 0.4772 *c* = 1.3025
	$NiCrO_3$	*D*5.1	*hR*10/1	5	5	–
	ZrO_2	*C*1	*cF*12/1	1	1	*a* = 0.5148
	Co_3O_4		*cF*56/3	11	13	*a* = 0.8126

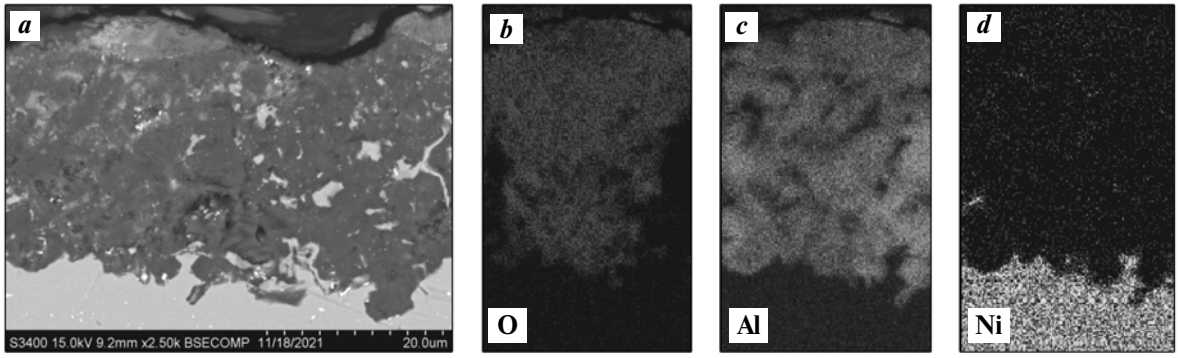

Fig. 5. SEM image of uncoated sample cross-section after annealing (***a***) and map of O (***b***), Al (***c***) and Ni (***d***) distribution in the oxidized layer

Рис. 5. РЭМ-изображение поперечного шлифа образца без покрытия после отжига (***a***) и карта распределения элементов в окисленном слое O (***b***), Al (***c***) и Ni (***d***)

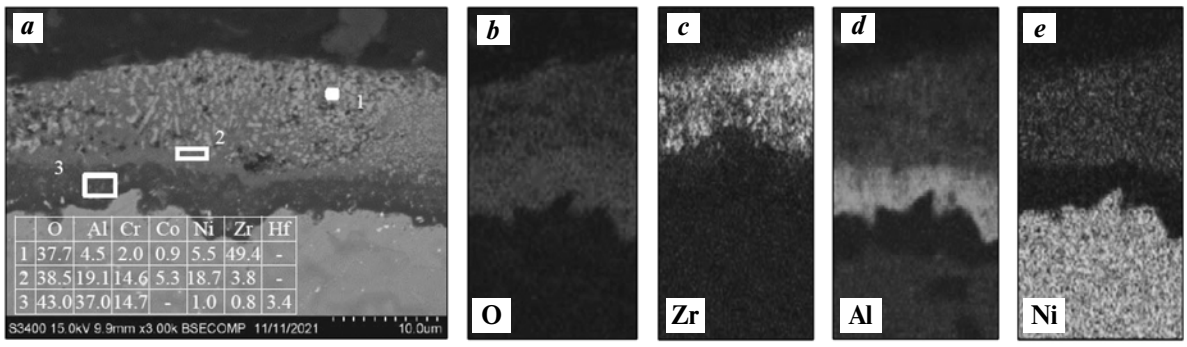

Fig. 6. SEM image of coating *4* cross-section after annealing with indicated EPMA areas (***a***) and map of O (***b***), Zr (***c***), Al (***d***), Ni (***e***) distribution in the oxidized layer

The insert indicates concentrations of elements (wt.%) in the indicated areas

Рис. 6. РЭМ-изображение поперечного шлифа покрытия *4* после отжига с указанием областей МРСА (***a***) и карта распределения элементов в окисленном слое O (***b***), Zr (***c***), Al (***d***), Ni (***e***)

На вставке приведены концентрации элементов (мас.%) в указанных областях

10 μm, which is three times less than for the uncoated sample.

Conclusions

1. We studied the formation of electrospark coatings on Ni-containing SLM alloys with zirconium electrodes. In high-energy modes ($\sum E$ = 5197÷17212 J), consistent cathode weight gain was observed. In low-energy modes ($\sum E$ = 1459÷2915 J) weight gain occurred during the first 1—4 minutes, while cathode weight decreased as the processing time increased.

2. We measured the ESD process variables in each mode: single pulse discharge energy, number of pulses, and total energy of pulsed discharges per 1 min. The coatings 15—30 μm thick with up to 100 % continuity reduce SLM sample surface roughness (R_a) by 1.3—2.8 time.

3. We found the formation of heat-resistant phases with $ZrNi_2Al$, ZrNi, $ZrCr_2$, and oxides ($Zr_3NiO(x)$, Zr(O,N)) in the ESD coatings as a result of interaction between zirconium and the dissolved oxygen present in the SLM samples.

4. The ESD coatings have 9.0—12.5 GPa hardness, and 122—145 GPa modulus of elasticity. Electrospark treatment improves the SLM alloy properties. The hardness is increased by 1.3—1.8 times, wear resistance, by 7.5—20 times, and oxidation resistance, by 10—20 %. In terms of its properties, the best coating was produced in low-energy mode with $\sum E$ = 2915 J.

Acknowledgments: *The research was funded by the Ministry of Science and Higher Education of the Russian Federation as part of the State assignment (Project 0718-2020-0034).*

Работа выполнена при финансовой поддержке Министерства науки и высшего образования РФ в рамках государственного задания (проект 0718-2020-0034).

References

1. *Каблов Е.Н.* Стратегические направления развития материалов и технологий их переработки на период до 2030 года. *Авиационные материалы и технологии.* 2012. No. S. С. 7—17.
   Kablov E.N. Strategical areas of developing materials and their processing technologies for the period up to 2030. *Aviatsionnye materialy i tekhnologii.* 2012. No. S. P. 7—17 (In Russ.).
2. *Логунов А.В., Берсенев А.Г., Логачёва А.И.* Проблемы и перспективы применения металлургии гранул для ракетно-космической техники. *Двигатель.* 2008. No. 2. С. 8—11.
   Logunov A.V., Bersenyev A.G., Logacheva A.I. Problems and prospects of application of metallurgy of pellets for rocket and space technology. *Dvigatel'.* 2008. No. 2. P. 8—11 (In Russ.).
3. *Kaplanskii Yu.Yu., Zaitsev A.A., Levashov E.A., Loginov P.A., Sentyurina Zh.A.* NiAl based alloy produced by HIP and SLM of pre-alloyed spherical powders. Evolution of the structure and mechanical behavior at high temperatures. *Mater. Sci. Eng. A.* 2018. Vol. 717. P. 48—59. DOI: 10.1016/j.msea.2018.01.057.
4. *Carter L.N., Martin Ch., Withers Ph. J., Attallah M.M.* The influence of the laser scan strategy on grain structure and cracking behaviour in SLM powder-bed fabricated nickel superalloy. *J. Alloys Compd.* 2014. Vol. 615. P. 338—347. DOI: 10.1016/j.jallcom.2014.06.172.
5. *Оспенникова О.Г.* Стратегия развития жаропрочных сплавов и сталей специального назначения, защитных и теплозащитных покрытий. *Авиационные материалы и технологии.* 2012. No. S. С. 19—36.
   Ospennikova O.G. Development strategics of high-temperature alloys and special steels, protective and thermoprotective coatings. *Aviatsionnye materialy i tekhnologii.* 2012. No. S. P. 19—36 (In Russ.).
6. *Поклад В.А., Шкретов Ю.П., Абраимов Н.В.* Покрытия для защиты от высокотемпературной газовой коррозии лопаток ротора турбины ГТД. *Двигатель.* 2010. No. 4 (70). С. 2—4.
   Poklad V.A., Shkretov Yu.P., Abraimov N.V. Coatings for protection against high-temperature gas corrosion of turbine turbine rotor blades. *Dvigatel'.* 2010. No. 4 (70). P. 2—4 (In Russ.).
7. *Хокинг М., Васантасри В., Сидки П.* Металлические и керамические покрытия: Получение, свойства и применение. М.: Мир, 2000.
   Khocking M., Vasantasri V., Sidki P. Metallic and ceramic coatings: Production, properties and applications. Moscow: Mir, 2000 (In Russ.).
8. *Подчерняева И.А., Панасюк А. Д., Тепленко М. А., Подольский В.И.* Защитные покрытия на жаропрочных никелевых сплавах (обзор). *Порошковая металлургия.* 2000. No. 9/10. С. 12—27.
   Podchernyaeva I.A., Panasyuk A.D., Teplenko M.A., Podol'skii V.I. Protective coatings on heat-resistant nickel al-

loys (Review). *Powder Metal. Met. Ceram*. 2000. Vol. 39. No. 9-10. P. 434—444.

9. *Матвеев П.В., Будиновский С.А., Мубояджян С.А., Косьмин А.А.* Защитные жаростойкие покрытия для сплавов на основе интерметаллидов никеля. *Авиационные материалы и технологии*. 2013. No. 2 (27). С. 12—15.
   Matveev P.V., Budinovsky S.A., Muboyajyan S.A., Kosmin A.A. Protective heat-resistant coatings for nickel intermetallic alloys. *Aviatsionnye materialy i tekhnologii*. 2013. No. 2 (27). P. 12—15 (In Russ.).
10. *Чубаров Д.А., Будиновский С.А., Смирнов А.А.* Магнетронный способ нанесения керамических слоев теплозащитных покрытий. *Авиационные материалы и технологии*. 2016. No. 4 (45). С. 23—30.
    Chubarov D.A., Budinovsky S.A., Smirnov A.A. Magnetron method of applying ceramic layers of heat-protective coatings. *Aviatsionnye materialy i tekhnologii*. 2016. No. 4 (45). P. 23—30 (In Russ.).
11. *Будиновский С.А., Чубаров Д.А., Матвеев П.В.* Современные способы нанесения теплозащитных покрытий на лопатки газотурбинных двигателей (обзор). *Авиационные материалы и технологии*. 2014. No. S5. С. 38—44.
    Budinovsky S.A., Chubarov D.A., Matveev P.V. Modern methods of applying heat-protective coatings to the blades of gas turbine engines (review). *Aviatsionnye materialy i tekhnologii*. 2014. No. S5. P. 38—44 (In Russ.).
12. *Абраимов Н.В., Елисеев Ю.С., Крымов В.В.* Авиационное материаловедение и технология обработки металлов Учеб. пособие для авиац. вузов. М.: Высш. шк., 1998.
    Abraimov N.V., Eliseev Yu.S., Krymov V.V. Aviation materials science and metal processing technology: Textbook. Moscow: Vysshaya shkola, 1998.
13. *Балдаев Л.Х., Балдаев С.Л., Мазилин И.В., Ахметгареева А.М.* Применение термобарьерных покрытий для лопаток современных газотурбинных установок на примере ГТД-110М. *Надежность и безопасность энергетики*. 2016. No. 2 (33). С. 70—72.
    Baldaev L.H., Baldaev S.L., Mazilin I.V., Akhmetgareeva A.M. Application of thermal barrier coatings for the blades of modern gas turbine units on the example of GTD-110M. *Nadezhnost' i bezopasnost' energetiki*. 2016. No. 2 (33). P. 70—72 (In Russ.).
14. *Денисова В.С., Соловьёва Г. А., Орлова Л.А.* Синтез ресурсных жаростойких эмалевых покрытий на основе стекол барийалюмосиликатной системы для никелевых сплавов. *Успехи в химии и химической технологии*. 2014. Т. 28. No. 8 (157). С. 39—42.
    Denisova V.S., Solovieva G.A., Orlova L.A. Synthesis of resource heat-resistant enamel coatings based on glasses of the barium aluminum silicate system for nickel alloys. *Uspekhi v khimii i khimicheskoy tekhnologii*. 2014. Vol. 28. No. 8 (157). P. 39—42 (In Russ.).
15. *Wang Mao-cai, Wang Wei-fu, Xie Yu-jiang, Zhang Jie.* Electro-spark epitaxial deposition of NiCoCrAlYTa alloy on directionally solidified nickel-based superalloy. *Trans. Nonferrous Met. Soc. China*. 2010. Vol. 20. Issue 5. P. 795—802.
16. *Enrique P. D., Marzbanrad E., Mahmoodkhani Y., Jiao Z., Toyserkani E., Zhou N.* Surface modification of binder-jet additive manufactured Inconel 625 via electrospark deposition. *Surf. Coat. Technol*. 2019. Vol. 362. P. 141—149.
17. *Левашов Е.А. Кудряшов А.Е., Замулаева Е.И., Погожев Ю.С., Санин В.Н., Андреев Д.Е., Юхвид В.И.* Особенности формирования, структура, состав и свойства электроискровых покрытий на никелевом сплаве ЖС6У при использовании сплава ХТН-61 СВС-Ц. *Известия вузов. Порошковая металлургия и функциональные покрытия*. 2009. No. 2. С. 33—38.
    Levashov E.A., Kudryashov A.E., Zamulaeva E.I., Pogozhev Y.S., Andreev D.E., Yukhvid V.I., Sanin V.N. Features of formation and the structure, composition, and properties of electrospark coatings on the ZhS6U nickel alloy with the use of the KhTN-61 SHS-Ts alloy. *Russ. J. Non-ferr. Met*. 2009. Vol. 50. No. 5. P. 534—539.
18. *Kudryashov A.E., Potanin A.Y., Lebedev D.N., Sukhorukova I.V., Shtansky D.V., Levashov E.A.* Structure and properties of Cr—Al—Si—B coatings produced by pulsed electrospark deposition on a nickel alloy. *Surf. Coat. Technol.* 2016. Vol. 285. P. 278—288.
19. *Kudryashov A.E., Lebedev D.N., Potanin A.Y., Levashov E.A.* Structure and properties of coatings produced by pulsed electrospark deposition on nickel alloy using Mo—Si—B electrodes. *Surf. Coat. Technol.* 2018. Vol. 335. P. 104—117.
20. *Kudryashov A.E., Kiryukhantsev-Korneev Ph.V., Petrzhik M.I., Levashov E.A.* Application of Zr—Si—B electrodes for electrospark alloying of Inconel 718 in vacuum, argon and air environment. *CIS Iron Steel Rev.* 2019. Vol. 18. P. 46—51.
21. *Цивирко Э.И., Лысенко Н.А., Клочихин В.Г., Жеманюк П.Д.* Легирование и модифицирование

никелевых сплавов цирконием. *Нові матеріали і технології в металургії та машинобудуванні*. 2007. No. 2. С. 22—29.

Tsyvirko E.I., Lysenko N.A., Klochikhin V.G., Zhemanyuk P.D. Alloying and modification of zirconium nickel alloys. *Novyye materialy i tekhnologii v metallurgii i mashinostroyenii*. 2007. No. 2. P. 22—29 (In Russ.).

22. *Базылева О.А., Аргинбаева Э.Г., Луцкая С.А.* Методы повышения коррозионной стойкости жаропрочных никелевых сплавов (обзор). *Труды ВИАМ*. 2018. No. 4 (64). С. 3—8.

Bazyleva O.A., Arginbaeva E.G., Lutskaya S.A. Ways of increasing corrosion resistance of superalloys (Review). *Trudy VIAM*. 2018. No. 4 (64). P. 3—8 (In Russ.).

23. *Верхотуров А.Д., Гордиенко П.С., Коневцов Л.А., Панин Е.С., Потапова Н.М.* Температурное окисление вольфрамокобальтовых твердых сплавов. *Перспективные материалы*. 2008. No. 2. С. 68—75.

Verkhoturov A.D., Gordiyenko P.S., Konevtsov L.A., Panin E.S., Potapova N.M. Temperature oxidation of tungsten-cobalt hard alloys. *Perspektivnye materialy*. 2008. No. 2. P. 68—75 (In Russ.).

24. *Вострикова Я.А., Верхотуров А.Д., Бурков А.А., Рыбалкин А.А., Коновалова Н.С.* Повышение жаростойкости и износостойкости вольфрамсодержащих твердых сплавов методом ЭИЛ. *Ученые записки Комсомольского-на-Амуре гос. техн. ун-та*. 2017. Т. 1. No. 2 (30). С. 90—99.

Vostrikov Ya.A., Verkhoturov A.D., Burkov A.A., Rybalkin A.A., Konovalova N.S. Increasing the heat resistance and wear resistance of hard tungsten alloys by spark alloying. *Uchenye zapiski Komsomol'skogo-na-Amure gosudarstvennogo tehnicheskogo universiteta*. 2017. Vol. 1. No. 2 (30). P. 90—99 (In Russ.).

25. *Wang X.-R., Wang Z.-Q., He P., Lin T.-S., Shi Y.* Microstructure and wear properties of CuNiSiTiZr high-entropy alloy coatings on TC11 titanium alloy produced by electrospark — computer numerical control deposition process. *Surf. Coat. Technol*. 2015. Vol. 283. P. 156—161. DOI: 10.1016/j.surfcoat.2015.10.013.

26. *Hong X., Tan Y., Zhou C., Xu T., Zhang Z.* Microstructure and tribological properties of Zr-based amorphous-nanocrystalline coatings deposited on the surface oftitanium alloys by Electrospark Deposition. *Appl. Surf. Sci.* 2015. Vol. 356. P. 1244—1251. DOI: 10.1016/j.apsusc.2015.08.233.

27. *Hong X., Tan Y., Wang X., Xu T., Gao L.* Microstructure and wear resistant performance of TiN/Zr-base amorphous-nanocrystalline composite coatings on titanium alloy by electrospark deposition. *Surf. Coat. Technol*. 2016. Vol. 305. P. 67—75. DOI: 10.1016/j.surfcoat.2016.07.077.

28. *Cadney S., Brochu M.* Formation of amorphous $Zr_{41,2}Ti_{13,8}Ni_{10}Cu_{12,5}Be_{22,5}$ coatings via the Electro-Spark Deposition process. *Intermetallics*. 2008. Vol. 16. P. 518—523. DOI: 10.1016/j.intermet.2007.12.013.

29. *Kuptsov K.A., Antonyuk M.N., Bondarev A.V., Sheveyko A.N., Shtansky D.V.* Electrospark deposition of wear and corrosion resistant Ta(Zr)C—(Fe,Mo,Ni) coatings to protect stainless steel from tribocorrosion in seawater. *Wear*. 2021. Vol. 486—487. Art. 204094. DOI: 10.1016/j.wear.2021.204094.

30. *Верхотуров А.Д., Подчерняева И.А., Прядко Л.Ф. Егоров Ф.Ф.* Электродные материалы для электроискрового легирования. М.: Наука, 1988.

Verkhoturov A.D., Podchernyayeva I.A., Pryadko L.F., Eegorov F.F. Electrode materials for electrospark alloying. Moscow: Nauka, 1988 (In Russ.).

31. *Николенко С.В., Верхотуров А.Д.* Новые электродные материалы для электроискрового легирования. Владивосток: Дальнаука, 2005.

Nikolenko S.V., Verkhoturov A.D. New electrode materials for electrospark alloying. Vladivostok: Dalnauka, 2005 (In Russ.).

32. *Федосеев М.Е., Кошуро В.А., Аман А., Фомин А.А.* Структура и твердость стали Х12МФ после электроискрового легирования цирконием и цементации в графитовой пасте. *Вестник Саратовского гос. техн. ун-та*. 2020. No. 2 (85). С. 85—90.

Fedoseev M.E., Koshuro V.A., Aman A., Fomin A.A. Structure and hardness of steel Kh12MF after electric spark alloying with zirconium and cementation in graphite paste. *Vestnik Saratovskogo gosudarstvennogo tekhnicheskogo universiteta*. 2020. No. 2 (85). P. 85—90 (In Russ.).

33. *Николенко С.В., Верхотуров А.Д., Коваленко С.В.* Поверхностная обработка титанового сплава ВТ-20 электроискровым легированием. *Перспективные материалы*. 2002. No. 3. С. 13—19.

Nikolenko S.V., Verkhoturov A.D., Kovalenko S.V. Surface treatment of titanium alloy VT-20 by electrospark alloying. *Perspektivnyye materialy*. 2002. No. 3. P. 13—19 (In Russ.).

34. *Николенко С.В., Ри Х.* Электродные материалы для электроискрового легирования с минеральными и

самофлюсующимися добавками. Хабаровск: ТОГУ, 2015.

Nikolenko S.V., Ri Kh. Electrode materials for electrospark alloying with mineral and self-fluxing additives. Khabarovsk: TOGU, 2015 (In Russ.).

35. *Zaitsev A.A., Sentyurina Zh.A, Levashov E.A., Pogozhev Y.S., Sanin V.N., Loginov P.A., Petrzhik, M.I.* Structure and properties of NiAl—Cr (Co, Hf) alloys prepared by centrifugal SHS casting. Pt. 1. Room temperature investigations. *Mater. Sci. Eng. A*. 2017. Vol. 690. P. 463—472.
36. *Горелик С.С., Скаков Ю.А., Расторгуев Л.Н.* Рентгенографический и электронно-оптический анализ. М.: МИСиС, 1994.

Gorelik S.S., Skakov Yu.A., Rastorguev L.N. Radiographic and electron-optical analysis. Moscow: MISIS, 1994 (In Russ.).
37. *Шелехов Е.В., Свиридова Т.А.* Программы для рентгеновского анализа поликристаллов. МиТОМ. 2000. No. 8. С. 16—19.

Shelekhov E.V., Sviridova T.A. Programs for *X*-ray analysis of polycrystals. *Metal Science Heat Treatment*. 2000. Vol. 42. P. 309—313.
38. *Levashov E.A., Shtansky D.V., Kiryukhantsev-Korneev Ph.V., Petrzhik M.I., Tyurina M.Ya., Sheveyko A.N.* Multifunctional nanostructured coatings: Formation, structure, and the uniformity of measuring their mechanical and tribological properties. *Russ. Metallurgy (Metally)*. Vol. 2010. No. 10. P. 917—935.
39. *Войтович Р.Ф., Пугач Э.А.* Окисление тугоплавких соединений: Справочник. Под ред. Г.В. Самсонова. Киев: Наук. Думка. 1968.

Voitovich R.F., Pugach E.A. Oxidation of refractory compounds: Handbook (Ed. G.V. Samsonov). Kiev: Naukova Dumka. 1968 (In Russ.).
40. Диаграммы состояния двойных металлических систем: Справочник. Под общ. ред. Н.П. Лякишева. Т. 2. М.: Машиностроение, 1997.

Diagrams of the state of double metal systems: Guide (Ed. N.P. Lyakishev). Vol. 2. Moscow: Mashinostroyenie, 1997 (In Russ.).
41. Диаграммы состояния двойных металлических систем: Справочник. Под общ. ред. Н.П. Лякишева. Т. 3. Кн. 1. М.: Машиностроение, 2001.

Diagrams of the state of double metal systems: Guide (Ed. N.P. Lyakishev). Vol. 3. Book 1. Moscow: Mashinostroyenie, 2001 (In Russ.).
42. *Дриц М.Е., Будберг П.Б.* Свойства элементов: Справочник. М.: Металлургия, 1985.

Drits M.E., Budberg P.B. Properties of elements': Guide. Moscow: Metallurgiya, 1985 (In Russ.).
43. *Sheveyko A.N., Kuptsov K.A., Kiryukhantsev-Korneev Ph.V., Kaplansky Yu.Yu., Orekhov A.S., Levashov E.A.* Protective coatings for LPBF Ni-based superalloys using a combination of electrospark deposition and pulsed arc evaporation methods. *Appl. Surf. Sci.* 2022. Vol. 581. Art. 152357. DOI: 10.1016/j.apsusc.2021.152357.
44. *Kiryukhantsev-Korneev Ph.V., Sheveyko A.N., Shvindina N.V., Levashov E.A., Shtansky D.V.* Comparative study of Ti—C—Ni—Al, Ti—C—Ni—Fe, and Ti—C—Ni—Al/Ti—C—Ni—Fe coatings produced by magnetron sputtering, electro-spark deposition, and a combined two-step process. *Ceram. Inter.* 2018. Vol. 44. Iss. 7. P. 7637—7646. https://www.sciencedirect.com/science/article/pii/S0272884218302025.
45. *Xian L., Zhao H., Xian G., Fan H., Xiong J.* Oxidation resistance and thermal insulation performance of thin nano-multilayered $(Al,Cr)_2O_3/ZrO_2$ coating prepared by arc ion plating technique. *Mater. Lett.* 2020. Vol. 281. Art. 128649. DOI: 10.1016/j.matlet.2020.128649.